Kinetics of the Reactions of *n*-Alkyl (C_2H_5, *n*-C_3H_7, and *n*-C_4H_9) Radicals with CH_3

Vadim D. Knyazev*,† and Irene R. Slagle*

The Catholic University of America, Department of Chemistry, Washington, DC 20064

Received: March 8, 2001; In Final Form: April 27, 2001

The ethyl-methyl, *n*-propyl-methyl, and *n*-butyl-methyl cross-radical reactions were studied by laser photolysis/photoionization mass spectroscopy. Overall rate constants were obtained in direct real-time experiments in the temperature region 297−800 K and bath gas (helium) density (3−36) × 10^{16} atom cm^{-3}. The observed overall $C_2H_5 + CH_3$ (1), *n*-$C_3H_7 + CH_3$ (2), and *n*-$C_4H_9 + CH_3$ (3) rate constants demonstrate negative temperature dependences. Master equation modeling of collisional effects indicates that the *n*-$C_3H_7 + CH_3$ and the *n*-$C_4H_9 + CH_3$ reactions are at the high-pressure limit under all experimental conditions used. The $C_2H_5 + CH_3$ reaction is not at the high-pressure limit and falloff in reaction 1 cannot be neglected at 800 K. Falloff corrections applied to reaction 1, on average, reach 45% at 800 K and introduce noticeable uncertainties in the extrapolated high-pressure-limit rate constant values. The following expressions for the high-pressure-limit rate constants of reaction 1−3 were obtained: $k_1^\infty = 2.36 \times 10^{-11} \exp(433\ K/T)$, $k_2^\infty = 3.06 \times 10^{-11} \exp(387\ K/T)$, and $k_3^\infty = 2.28 \times 10^{-11} \exp(473\ K/T)$ cm^3 $molecule^{-1}$ s^{-1}. C_3H_8 was detected as a product of reaction 1 and C_5H_{12} and C_4H_8 were detected as products of reaction 3.

I. Introduction

Radical−radical cross-combination reactions constitute an integral part of the overall mechanisms of oxidation and pyrolysis of hydrocarbons.[1,2] Reliable rate and branching data on this type of reaction are sparse as these reactions are difficult to study experimentally due to the high reactivity of the chemical species involved. Because of the lack of directly obtained experimental values, rate constants of cross-combination reactions are often estimated using the "geometric mean rule"[3−5]

$$k_{AB} = 2(k_{AA}k_{BB})^{1/2} \qquad \text{(I)}$$

(Here, k_{AB} is the rate constant of the A + B reaction and k_{AA} and k_{BB} are the rate constants of the A + A and B + B self-reactions, respectively.) Validation of the geometric mean rule, however, is also problematic for the same reason, i.e., a deficit of directly obtained experimental rate constant values.

Recently, we have experimentally determined the rate constants of the reactions of two delocalized radicals (allyl and propargyl) with CH_3.[6] In the current study, we report the results of an experimental investigation of three reactions of *n*-alkyl radicals with CH_3

$$C_2H_5 + CH_3 \rightarrow \text{products (301−800 K)} \qquad (1)$$

$$n\text{-}C_3H_7 + CH_3 \rightarrow \text{products (297−600 K)} \qquad (2)$$

$$n\text{-}C_4H_9 + CH_3 \rightarrow \text{products (301−520 K)} \qquad (3)$$

Reactions 1−3 were studied by means of Laser Photolysis/Photoionization Mass Spectrometry at low bath gas densities ([He] = (3−36) × 10^{16} atom cm^{-3}). Overall rate constants were obtained in direct experiments by monitoring the real-time kinetics of both the R (R = C_2H_5, *n*-C_3H_7, or *n*-C_4H_9) and the CH_3 radical. Temperature intervals for each of the reactions are indicated in parentheses.

Reaction 1 is the only one for which absolute experimental values of the rate constant have been reported.[5,7,8] All previous measurements were performed only at room temperature and the reported values of the rate constant differ by as much as a factor of 2. Anastasi and Arthur[7] used molecular modulation spectrometry at a pressure of 131 Torr of nitrogen/azomethane/azoethane bath gas and obtained the value of $k_1 = (4.7 \pm 0.4) \times 10^{-11}$ cm^3 $molecule^{-1}$ s^{-1}. Garland and Bayes[5] applied the Laser Photolysis/Photoionization Mass Spectrometry technique and reported the room-temperature rate constant of reaction 1 at 4 Torr of helium and argon bath gases, $k_1 = (9.3 \pm 4.2) \times 10^{-11}$ cm^3 $molecule^{-1}$ s^{-1}. Sillesen et al. used pulsed radiolysis of H_2 with spectroscopic detection of CH_3 and kinetic modeling to study the system of reactions $H + C_2H_4 \rightarrow C_2H_5$, $H + C_2H_5 \rightarrow 2CH_3$, $C_2H_5 + CH_3 \rightarrow$ products. The value of $k_1 = (6.6 \pm 0.3) \times 10^{-11}$ cm^3 $molecule^{-1}$ s^{-1} was derived by these authors from modeling [CH_3] vs time profiles using an assumed chemical mechanism and literature values of the rate constants of the other involved reactions.

This article is organized as follows. Section I is an introduction. Section II presents the experimental method and the results. Falloff modeling is described in section III and a discussion is given in section IV.

II. Experimental Section

In this section, the experimental apparatus used is described and the photolysis routes of the free radical precursors are characterized. The method of determination of rate constants and the associated kinetic mechanism is explained next, followed by a detailed description of the experimental procedure used. Finally, the experimental results are presented.

Apparatus. Details of the experimental apparatus[9] and method[10] have been described previously. Only a brief description is presented here. Pulsed 193 nm unfocused collimated radiation from a Lambda Physik 201 MSC ArF excimer laser

† E-Mail: knyazev@cua.edu.

10.1021/jp010878s CCC: $20.00
Published on Web 06/13/2001

was directed along the axis of a 50 cm-long 1.05 cm i.d. heatable tubular quartz reactor coated with boron oxide or poly(dimethylsiloxane).[11] The laser was operated at 4 Hz and at a fluence of 80−165 mJ/pulse. The energy flux of the laser radiation inside the reactor was in the range of 4−17 mJ/cm^2 per pulse depending on the degree of laser beam attenuation.

Gas flowing through the tube at ∼4 m s^{-1} (to replace the photolyzed gas with a fresh reactant gas mixture between the laser pulses) contained free radical precursors in low concentrations and the bath gas, helium. The gas was continuously sampled through a 0.04 cm-diameter tapered hole in the wall of the reactor (gas-sampling orifice) and formed into a beam by a conical skimmer before it entered the vacuum chamber containing the photoionization mass spectrometer (PIMS). As the gas beam traversed the ion source, a portion was photoionized using an atomic resonance lamp, mass selected in an EXTREL quadrupole mass filter, and detected by a Daly detector.[12] Temporal ion signal profiles were recorded from 10 to 30 ms before each laser pulse to 15−35 ms following the pulse by using an EG&G ORTEC multichannel scaler interfaced with a PC computer. Typically, data from 1000 to 15000 repetitions of the experiment were accumulated before the data were analyzed. The sources of ionizing radiation were chlorine (8.9−9.1 eV, CaF_2 window, used to detect C_2H_5, *n*-C_3H_7, and *n*-C_4H_9), hydrogen (10.2 eV, MgF_2 window, used to detect CH_3, C_3H_6, C_4H_8, $(CH_3)_2CO$, $(C_2H_5)_2CO$, (*n*-C_3H_7)$_2$CO, and *n*-C_4H_9-Br), and argon (11.6−11.9 eV, LiF window, used to detect C_2H_4, C_3H_8, and C_5H_{12}) resonance lamps.

Photolysis of Radical Precursors. Radicals were produced by the 193 nm photolysis of corresponding precursors. The photolysis of acetone at 193 nm, which was used in this study as the source of methyl radicals, was shown by Lightfoot et al.[13] to proceed predominantly (>95%) via channel 4a under conditions similar to those used in the current work

$$CH_3C(O)CH_3 \xrightarrow{193\ nm} 2CH_3 + CO \quad (4a)$$

$$\rightarrow H + CH_2C(O)CH_3 \quad (4b)$$

$$\rightarrow CH_4 + CH_2CO \quad (4c)$$

Photolysis channels 4b and 4c are known[13] to occur to a minor degree, < 3% and < 2%, respectively. The initial concentration of CH_3 radicals produced by the photolysis can thus be determined by measuring the photolytic depletion of $CH_3C(O)CH_3$ (the fraction of acetone decomposed due to photolysis) using time-resolved photoionization mass spectrometry (see below).

Ethyl, *n*-propyl, and *n*-butyl radicals were produced by the photolysis of diethyl ketone,[14] 4-heptanone,[15] and 1-bromobutane,[16] respectively

$$(C_2H_5)_2CO \xrightarrow{193\ nm} 2\ C_2H_5 + CO \quad (5a)$$

$$\rightarrow \text{other products} \quad (5b)$$

$$CH_3CH_2CH_2C(O)CH_2CH_2CH_3 \xrightarrow{193\ nm} 2\ n\text{-}C_3H_7 + CO \quad (6a)$$

$$\rightarrow \text{other products} \quad (6b)$$

$$n\text{-}C_4H_9Br \xrightarrow{193\ nm} n\text{-}C_4H_9 + Br \quad (7a)$$

$$\rightarrow \text{other products} \quad (7b)$$

Radical precursors were obtained from Aldrich (acetone (>99.9%), diethyl ketone (>99%), 4-heptanone (98%), and 1-bromobutane (>99%)) and were purified by vacuum distillation prior to use. Helium (>99.999%, <1.5 ppm of O_2, MG Industries) was used without further purification.

Method of Determination of Rate Constants. CH_3 and R radicals (R = C_2H_5, *n*-C_3H_7, or *n*-C_4H_9) were produced simultaneously by the 193 nm photolysis of a mixture of corresponding precursors highly diluted in the helium carrier gas (> 99.9%). The rate constant measurements were performed using a technique analogous to that applied by Niiranen and Gutman to the studies of the $SiH_3 + CH_3$ and $Si(CH_3)_3 + CH_3$ kinetics,[17] which is a further development of the method used by Garland and Bayes to study a series of radical cross-combination reactions.[5] Experimental conditions (in particular, the two precursor concentrations) were selected to create a large excess of initial concentrations of methyl radicals over the total combined concentration of all the remaining radicals formed in the system. The initial concentration of methyl radicals was always 22−88 times higher than that of R. The concentration of R radicals was always less than 1.8×10^{11} molecules cm^{-3}. Under these conditions, the self-recombination of methyl radicals was essentially unperturbed by the presence of the other radicals. At the same time, the kinetics of R decay was completely determined by the reaction with CH_3 and unaffected either by self-reaction or by reactions with other active species formed in the system, such as the side products of precursor photolysis.

Heterogeneous loss was the only additional sink of methyl and R radicals that had to be taken into account. Thus, the kinetic mechanism of the important loss processes of CH_3 and R in these experiments is as follows

$$R + CH_3 \rightarrow \text{products} \quad (1, 2, \text{or } 3)$$

$$CH_3 + CH_3 \rightarrow C_2H_6 \quad (8)$$

$$R \rightarrow \text{heterogeneous loss} \quad (9, 10, \text{or } 11)$$

$$CH_3 \rightarrow \text{heterogeneous loss} \quad (12)$$

(Here, reactions 9, 10, and 11 are the wall losses of C_2H_5, *n*-C_3H_7, and *n*-C_4H_9, respectively). For this mechanism and for the initial conditions described above, the system of first order differential equations can be solved analytically

$$\frac{[CH_3]_t}{[CH_3]_0} = \frac{k_{12}\exp(-k_{12}t)}{2k_8[CH_3]_0(1-\exp(-k_{12}t)) + k_{12}} \quad (II)$$

$$\frac{[R]_t}{[R]_0} = \exp(-k_w t)\left[\frac{k_{12}}{2k_8[CH_3]_0(1-\exp(-k_{12}t)) + k_{12}}\right]^{\frac{k_R[CH_3]_0}{2k_8[CH_3]_0}} \quad (III)$$

The variables k_R and k_W in eq III have the meanings of the rate constant of the R + CH_3 reaction ($k_R = k_1$, k_2, or k_3) and that of the R radical wall loss ($k_W = k_9$, k_{10}, or k_{11}).

Experimental signal profiles of CH_3 and R radicals (see subsection Procedure below) were fitted with eqs II and III, respectively, to obtain the values of the $k_8[CH_3]_0$ and $k_R[CH_3]_0$ products. The k_R rate constants ($k_R = k_1$, k_2, or k_3) were then obtained by dividing the experimental $k_R[CH_3]_0$ values by $[CH_3]_0$ determined by measuring the photolytic depletion of acetone

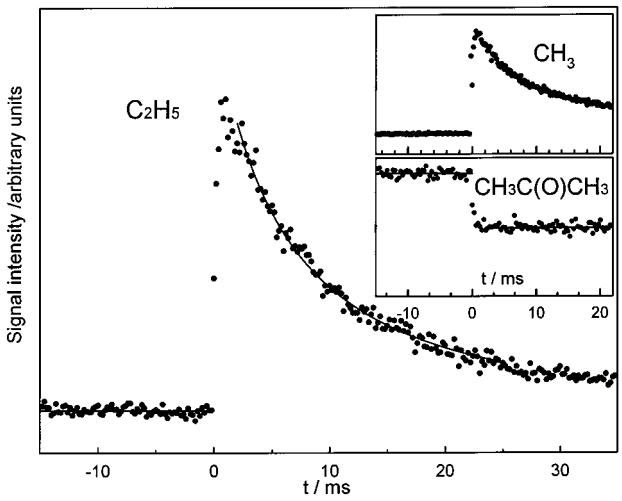

Figure 1. Examples of temporal ion signal profiles obtained in the experiments to measure k_1. $T = 600$ K, [He] $= 1.20 \times 10^{17}$ atoms cm^{-3}, [$(C_2H_5)_2CO$] $= 7.81 \times 10^{11}$ molecules cm^{-3}, [$CH_3C(O)CH_3$] $= 1.25 \times 10^{13}$ molecules cm^{-3}, [C_2H_5]$_0 \leq 1.08 \times 10^{11}$ molecules cm^{-3}, [CH_3]$_0 = 3.44 \times 10^{12}$ molecules cm^{-3}. Lines are the results of fits with formulas II (for CH_3) and III (for C_2H_5).

(see below). An important feature of this method is that exact knowledge of the initial concentration of R is not required for the determination of the rate constants. In this respect, the approach is similar to the pseudo-first-order method frequently applied to studies of kinetics of second-order reactions.

Procedure. In experiments with only one of the radical precursors present in the reactor under conditions where radical−radical reactions are negligible (low precursor concentration and/or low laser intensity), the radical kinetics (CH_3, C_2H_5, n-C_3H_7, or n-C_4H_9) was that of purely exponential decay. The rate of the decay did not depend on the concentration of the precursor or the laser intensity but was affected by the wall conditions of the reactor (such as coating and history of exposure to reactive mixtures). This decay was attributed to heterogeneous loss processes. The rate constants of heterogeneous loss of methyl (k_{12}) and R ($k_W = k_9$, k_{10}, or k_{11}) radicals were determined in separate sets of measurements. The wall loss rates of the C_2H_5, n-C_3H_7, and n-C_4H_9 radicals were in the ranges 3−28, 6−39, and 8−23 s^{-1}, respectively, and were minor compared to the rates of radical decay due to the reactions under study (1, 2, and 3). The wall loss rate constant of CH_3 decay was in the range 0−13 s^{-1}.

In the experiments to measure the R + CH_3 reaction rate constants, the initial (high) concentration of methyl radicals was determined by measuring the photolytic depletion of acetone (the fraction of acetone decomposed due to photolysis). The value of the decomposition ratio (the relative decrease in the precursor concentration upon photolysis) was obtained directly from the acetone ion signal profile (Typical profiles are shown in Figure 1.) and corrected for the ion signal background. The background (less than 10% of the acetone signal) was mainly due to a low, constant concentration of acetone molecules in the mass-spectrometer vacuum chamber and the interaction of the scattered UV light from the resonance lamp with the high voltage target of the Daly detector. The method of correction for the ion signal background is described in detail in ref 10. Initial concentrations of R (R = C_2H_5, n-C_3H_7, or n-C_4H_9) were evaluated by monitoring the photolytic depletion of corresponding precursors. Since products other than R were also produced in the photolysis (reactions 5−7), only upper limit values to the concentration of R could be obtained.

The procedure of determination of the R + CH_3 rate constants for each set of experimental conditions consisted of the following sequence of measurements:

1. Kinetics of heterogeneous loss of R (determination of k_W). Only the R radical precursor is present in the reactor (along with the helium carrier gas which is always present).

2. Decomposition ratio of the R radical precursor (determination of an upper limit of [R]$_0$).

3. Kinetics of heterogeneous loss of CH_3 (determination of k_{12}). Only acetone is in the reactor. The photolyzing laser beam is significantly attenuated to provide low CH_3 concentrations.

4. Decomposition ratio of acetone (determination of [CH_3]$_0$). Both radical precursors are in the reactor, from here to step 6. Low or no attenuation of the laser bean is used (high CH_3 concentrations), from here to step 6.

5. Kinetics of methyl radical decay (determination of the k_8[CH_3]$_0$ product).

6. Kinetics of R radical decay in the presence of methyl radicals (determination of the k_R[CH_3]$_0$ product and k_R.

Measurements 4 and 5 were repeated in reverse order after monitoring the kinetics of R radicals in the presence of methyl radicals in order to ensure the stability of initial concentrations of CH_3. Also, the stability of the heterogeneous loss rate constants during the set of measurements was checked experimentally.

Typical temporal profiles of [$CH_3C(O)CH_3$] (photolytic precursor of CH_3 radicals), [CH_3], and [R] are shown in Figure 1 for R = C_2H_5. The lines through the experimental [CH_3] and [C_2H_5] vs time profiles are obtained from fits of these dependences with expressions II and III, respectively. In each experiment (consisting of the set of measurements described above), the value of the k_8[CH_3]$_0$ product was obtained from the fit of the [CH_3] vs time dependence (measured in step 5) using the value of k_{12} (wall loss of CH_3) determined in step 3. Then the value of the k_R[CH_3]$_0$ product was obtained from the fit of the [R] vs time dependence using the k_W, k_{12}, and k_8[CH_3]$_0$ values obtained in steps 1, 3, and 5, respectively. Finally, the value of k_R ($k_R = k_1$, k_2, or k_3) was obtained by dividing the k_R[CH_3]$_0$ product by [CH_3]$_0$ determined in step 4.

The sources of error in the measured experimental parameters such as temperature, pressure, flow rate, signal count, and so forth were subdivided into statistical and systematic and propagated to the final values of the rate constants using different mathematical procedures for propagating systematic and statistical uncertainties.[18] In particular, the effects of uncertainties in the heterogeneous radical decay rates and in the k_8[CH_3]$_0$ product on the derived k_1, k_2, and k_3 values were evaluated for all experiments. The error limits of the experimentally obtained rate constant values reported in this work represent a sum of 2σ statistical uncertainty and estimated systematic uncertainty.

Experimental Results. The rate constants of reaction 1 (k_1) were determined at temperatures between 301 and 800 K and bath gas densities [He] $= (3-12) \times 10^{16}$ atom cm^{-3}. The values of k_2 and k_3 were obtained at temperatures between 297 and 600 K and bath gas densities [He] $= (3-36) \times 10^{16}$ atom cm^{-3}. The upper limits of the experimental temperatures were determined by the onsets of thermal decomposition of C_2H_5,[19] n-C_3H_7,[15] and n-C_4H_9[16] radicals. Conditions and results of all experiments are listed in Table 1. It was verified experimentally that these rate constants did not depend on the photolyzing laser intensity, initial concentrations of R and CH_3, or reactor wall coating. The rate constants of reactions 1, 2, and 3 did not demonstrate any pressure dependence within the experimental uncertainties.

TABLE 1: Conditions and Results of Experiments to Determine the Rate Constants k_R of the R + CH_3 Reactions (R = C_2H_5, *n*-C_3H_7, or *n*-C_4H_9; $k_R = k_1$, k_2, or k_3)

T/K	[He][a]	[prec][b]	[C_3H_6O][b]	[R]$_0$[b]	[CH_3]$_0$[b]	I[c]	k_W/s^{-1}	k_{12}/s^{-1}	k_8[d]	k_R[d]	k/k^∞[e]	k_R^∞[d,f]	*F*[f]
						R = C_2H_5; $k_R = k_1$							
301	12.0	6.43	307.4	0.64	56.2	16	8.6[g]	7.5[g]	4.69 ± 1.80	9.65 ± 3.27	1.00	9.65	1.35
301	12.0	6.43	85.2	0.64	15.5	16	8.6	7.5	4.95 ± 1.39	9.98 ± 1.92	1.00	9.98	1.20
301	12.0	7.45	312.4	0.30	25.9	8	5.0	4.3	4.09 ± 1.29	10.44 ± 2.56	1.00	10.44	1.25
303	12.0	4.96	149.0	0.55	29.5	16	4.1	6.5	5.03 ± 1.71	9.19 ± 2.66	1.00	9.19	1.30
400	12.0	7.81	153.7	1.26	35.7	16	3.4	4.7	4.11 ± 1.30	7.26 ± 2.08	0.99	7.32	1.31
400	12.0	7.81	143.4	0.65	17.3	8	3.4	4.7	4.12 ± 1.19	7.07 ± 1.52	0.99	7.13	1.24
600	12.0	6.73	125.0	1.08	34.4	16	18.9	10.5	1.84 ± 0.55	4.47 ± 0.91	0.93	4.82	1.35
800	12.0	6.73	242.8	1.20	84.2	17	27.8	7.2	1.02 ± 0.17	2.98 ± 0.35	0.75	3.99	1.47
800	12.0	5.64	237.5	0.37	25.6	5	27.8	7.2	1.01 ± 0.32	2.79 ± 0.53	0.75	3.73	1.57
800	3.0	6.43	113.0	0.96	40.0	13	21.7	12.5	0.74 ± 0.21	2.52 ± 0.50	0.57	4.38	1.80
						R = *n*-C_3H_7; $k_R = k_2$							
297	12.0	46.1	268.5	0.98	36.4	13	8.9	4.8	4.33 ± 1.39	11.51 ± 2.82	1.00	11.51	1.25
301	12.0	31.6	297.6	0.69	24.8	8	6.2[g]	4.3[g]	4.12 ± 1.05	10.77 ± 2.08	1.00	10.77	1.19
304	12.0	22.5	72.95	0.48	10.8	13	8.6	7.1	4.56 ± 1.78	11.22 ± 2.58	1.00	11.22	1.23
340	12.0	14.3	317.8	0.90	42.8	9	6.4	0.0	3.80 ± 1.27	9.56 ± 2.88	1.00	9.56	1.30
340	12.0	14.3	173.7	0.90	23.4	9	6.4	0.0	3.70 ± 1.10	8.66 ± 1.32	1.00	8.66	1.15
440	12.0	14.9	367.7	1.29	60.5	8	7.1	0.2	2.99 ± 0.91	8.12 ± 2.04	1.00	8.12	1.25
440	12.0	14.9	377.4	0.65	30.4	4	7.1	0.2	2.91 ± 0.81	7.63 ± 1.77	1.00	7.63	1.23
600	3.0	9.75	277.5	1.35	60.4	12	11.8	5.3	1.16 ± 0.26	5.65 ± 1.09	0.99	5.73	1.21
600	36.0	10.3	260.7	1.19	53.2	12	38.6	0.0	2.44 ± 1.07	5.56 ± 1.67	1.00	5.56	1.30
						R = *n*-C_4H_9; $k_R = k_3$							
297	12.0	69.2	265.9	0.98	36.9	13	23.4	4.8	3.70 ± 1.41	11.10 ± 2.89	1.00	11.10	1.26
301	12.0	68.9	295.4	0.60	29.5	8	7.8[g]	4.3[g]	4.03 ± 1.10	9.59 ± 2.23	1.00	9.59	1.23
304	12.0	22.5	71.6	0.32	10.7	13	8.6	7.1	3.82 ± 1.71	12.34 ± 3.44	1.00	12.34	1.28
340	12.0	97.1	357.4	1.25	43.0	10	22.0	0.5	3.92 ± 1.17	9.71 ± 2.52	1.00	9.71	1.26
340	12.0	97.1	364.7	0.69	24.2	5	22.0	0.5	3.55 ± 1.00	8.62 ± 2.23	1.00	8.62	1.26
440	12.0	65.7	365.8	0.98	57.0	8	12.3	0.2	3.23 ± 0.99	7.14 ± 1.95	1.00	7.14	1.27
520	3.0	88.8	280.8	1.36	61.0	13	12.1	5.3	1.69 ± 0.44	5.12 ± 1.17	1.00	5.12	1.23
520	36.0	134.2	260.2	1.78	52.6	12	12.2	0.0	3.26 ± 0.88	5.93 ± 1.98	1.00	5.93	1.33

[a] Concentration of the bath gas (helium) in units of 10^{16} atom cm^{-3}. [b] Concentrations of the R radical photolytic precursor, acetone, R, and CH_3 in units of 10^{11} molecules cm^{-3}. Concentration of R is an upper limit (see text). [c] Laser intensity in mJ pulse^{-1} cm^{-2}. [d] In units of 10^{-11} cm^3 molecule^{-1} s^{-1}. [e] Calculated falloff correction factor (section III). [f] k_R^∞ are obtained by dividing the experimental k_R values by the calculated k/k^∞ factors. *F* is the uncertainty factor of k_R^∞ (i.e., upper and lower limiting values of k_R^∞ can be obtained by multiplying or dividing the optimum value by *F*). For reaction 1 (and reaction 2 at 600 K and [He] = 3.0×10^{16} atom cm^{-3}), the uncertainty factor includes the estimated uncertainty of extrapolation to the high pressure limit and the experimental uncertainty. For all other measurements, *F* includes only the experimental uncertainty. [g] Poly(dimethylsiloxane) reactor wall coating was used. Boron oxide coated reactor was used in all other experiments.

Although the measurement of k_8 (CH_3 recombination) was not the goal of the current work, the experiments provided rate constant values for the $CH_3 + CH_3$ reaction. Uncertainty in the k_8 values (Table 1) is rather high, up to 45% of the values, due to the fact that the experimental conditions were optimized for most accurate determination of k_R ($k_R = k_1$, k_2, or k_3), not k_8. The results obtained are in good agreement with those previously measured.[6,10,20]

Arrhenius plots of the rate constants of reaction 1−3 are shown in Figures 2 − 4. The observed rate constants decrease with increasing temperature. These temperature dependences can be represented with parametric fits given by the following expressions

$$k_1 = 2.61 \times 10^{-5} T^{-2.00} \exp(-332\ \mathrm{K}/T)\ \mathrm{cm^3\ molecule^{-1}\ s^{-1}} \quad \text{(IV)}$$

$$k_2 = 3.02 \times 10^{-11} \exp(391\ \mathrm{K}/T)\ \mathrm{cm^3\ molecule^{-1}\ s^{-1}} \quad \text{(V)}$$

$$k_3 = 2.28 \times 10^{-11} \exp(473\ \mathrm{K}/T)\ \mathrm{cm^3\ molecule^{-1}\ s^{-1}} \quad \text{(VI)}$$

The estimated uncertainties of these expressions are 25%. Experimental error limits of individual data points are given in Table 1.

C_3H_8 was detected as a product of reaction 1 and C_5H_{12} and C_4H_8 were detected as products of reaction 3, with product rise times matching those of the C_2H_5 and *n*-C_4H_9 decays. Attempts to detect the C_2H_4 product of the disproportionation channel of the $C_2H_5 + CH_3$ reaction were unsuccessful. The potential signal from C_2H_4 due to reaction 1 was obscured by the signal of ethylene that was observed in the absence of C_2H_5 radicals as a minor product of reactions following the photolysis of acetone. A similar formation of minor amounts of ethylene in the reactive system of the 193 nm photolysis of acetone was investigated by Lightfoot et al.[13] These authors attributed the effect of ethylene formation to the reaction of CH_2 (formed in the photolysis of a methyl radical produced in reaction 4 with both reaction 4 and the CH_3 photolysis occurring during the same laser pulse) with CH_3: $CH_2 + CH_3 \rightarrow C_2H_4 + H$.

Formation of the expected C_4H_{10} product of reaction 2 could not be monitored because the mass of C_4H_{10} (58) coincides with that of acetone. The signal of the C_3H_6 potential product of reaction 2 was obscured by that of the propene formed in the photolysis of 4-heptanone, reaction 6. The resultant temporal profile of the C_3H_6 signal consisted of two components, one appearing immediately following the photolyzing laser pulse (attributed to the photolysis of 4-heptanone) and a slower rising part that could be attributed to the disproportionation channel of reaction 2. However, these two components of the C_3H_6 signal could not be meaningfully resolved.

III. Falloff Effects

Experimental data on reactions 1−3 were obtained at low bath gas pressures, where falloff can be of importance. This section describes the assessment of pressure effects (falloff from

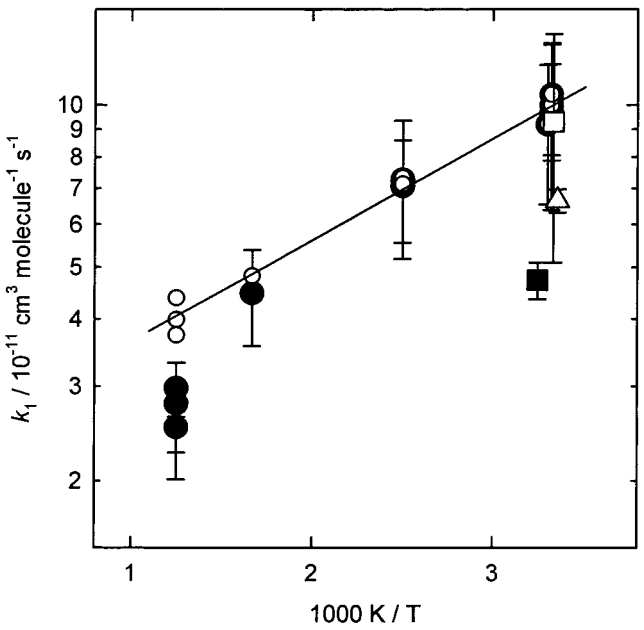

Figure 2. Temperature dependences of the experimentally obtained values of k_1 (filled circles) and extrapolated values of k_1^∞ (open smaller circles). At low temperatures, where k_1 and k_1^∞ coincide, open small circles are superimposed on the larger filled circles. Filled square, open square, and triangle represent the room-temperature k_1 values reported by Anastasi and Arthur,[7] Garland and Bayes,[5] and Sillesen et al.,[8] respectively. Solid line is the Arrhenius fit of the $k_1^\infty(T)$ dependence given by formula IX.

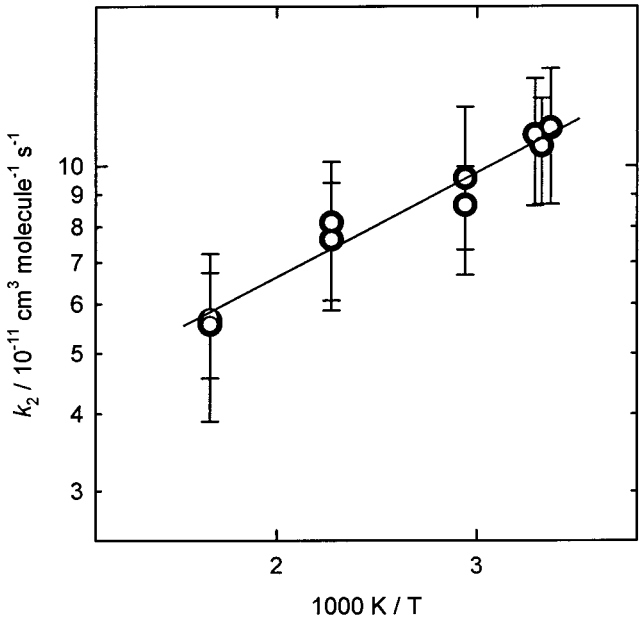

Figure 3. Temperature dependences of the experimentally obtained values of k_2 (filled circles) and extrapolated values of k_2^∞ (open smaller circles). Near coincidence of the filled and the open circles (open small circles are superimposed on the larger filled circles) demonstrates that reaction 2 is at the high-pressure limit under the conditions of all experiments except for a 1% deviation at 600 K and [He] = 3×10^{16} atom cm^{-3}. Solid line is the Arrhenius fit of the $k_2^\infty(T)$ dependence given by formula X.

the high-pressure limit) for reactions 1 and 2. It is demonstrated that although reaction 1 is in the falloff at the two highest experimental temperatures (600 and 800 K), reaction 2 is at the high-pressure limit under all experimental conditions. Because reaction 3 involves even larger molecules than reaction 2, it is expected to be at the high-pressure limit as well.

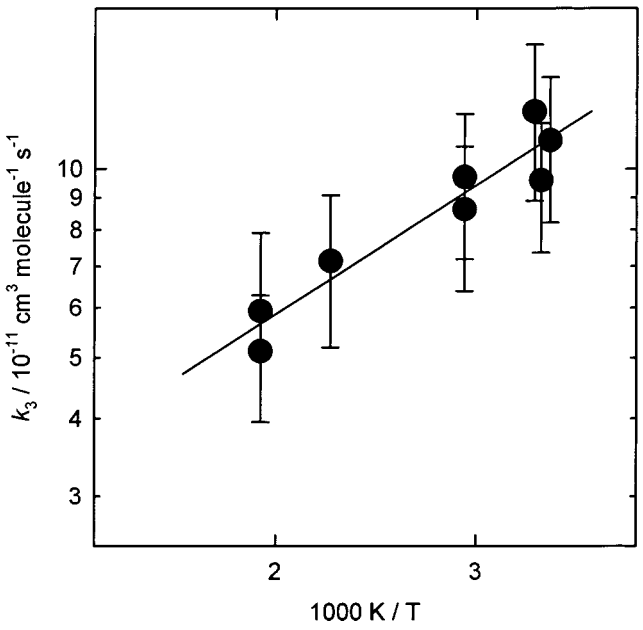

Figure 4. Temperature dependences of the experimentally obtained values of k_3. Solid line is the Arrhenius fit of the $k_3^\infty(T)$ dependence given by formula VI.

Approximate values of the microscopic energy-dependent rate constants $k_d(E)$ for decomposition of the R−CH_3 adducts were obtained using a method based on the inverse Laplace transform of the temperature dependence of the high-pressure-limit recombination rate ($k^\infty(T)$). In our earlier article,[6] the formula

$$k_d(E) = A_r^\infty B_{AB}^i \left(\frac{2\pi\mu}{h^2}\right)^{3/2} \frac{\rho_P(E - E_0 - E_r^\infty)}{\rho_{AB}(E)} \qquad \text{(VII)}$$

was derived. Here, A_r^∞ and E_r^∞ are the parameters of the modified Arrhenius equation

$$k_r^\infty = A_r^\infty (k_B T)^{-1/2} \exp\left(-\frac{E_r^\infty}{k_B T}\right) \qquad \text{(VIII)}$$

describing the temperature dependence of the high-pressure-limit A + B → AB recombination rate constant, μ is the reduced mass, E_0 is the energy barrier for adduct decomposition, B_{AB}^i is the rotational constant of the inactive[21−24] two-dimensional rotation of the AB adduct (with symmetry factor incorporated), and $\rho_{AB}(E)$ and $\rho_P(E)$ are the density-of-states functions of the adduct and of the pseudo-molecule formed by a combination of internal degrees of freedom (including overall rotations) of the A and B reactants.

Calculations of the falloff corrections performed in the current work exactly follow the iterative procedure of master equation modeling of ref 6, and thus, only a limited description of the procedure is presented here. Falloff factors (k/k^∞) were calculated for each experimental data point using the solution of the master equation. The properties of the model were selected in an iterative process. First, the experimentally obtained $k_r(T)$ temperature dependences (Figures 2 and 3) were assumed to represent those of the high-pressure-limit and were fitted with expression VIII. The A_r^∞ and E_r^∞ parameters thus obtained were used to evaluate the $k(E)$ functions. These $k(E)$ dependences were then used in master equation modeling which, in turn, yielded the calculated k/k^∞ falloff factors. The experimental $k_r(T)$ values were next divided by these k/k^∞ falloff factors to obtain the "corrected" high-pressure-limit rate constants. The

TABLE 2: Properties of Molecules Used in Models of Reactions 1, 2, and 3

	enthalpies of formation (kJ mol^{-1})	
	$\Delta_fH^0_{298}(C_2H_5) = 121.0 \pm 1.5$[14,25,26]	$\Delta_fH^0_{298}(n\text{-}C_3H_7) = 100.8 \pm 2.1$[27]
	$\Delta_fH^0_{298}(CH_3) = 146.0 \pm 1.0$[28,29]	$\Delta_fH^0_{298}(C_3H_8) = -104.7 \pm 0.5$[30]
	$\Delta_fH^0_{298}(n\text{-}C_4H_9) = 80.9 \pm 2.2$[27]	$\Delta_fH^0_{298}(n\text{-}C_4H_{10}) = -127.1 \pm 0.7$[31]
	$\Delta_fH^0_{298}(n\text{-}C_5H_{12}) = -146.8 \pm 0.6$[57]	
	vibrational frequencies (cm^{-1})	
C_2H_5:[a]	3114, 3036, 2987, 2920, 2844, 1442, 1442, 1383, 1369, 1133, 1185, 1025, 783, 532	
n-C_3H_7:[b]	3309, 3192, 3158, 3152, 3085, 3062, 3008, 1498, 1490, 1478, 1461, 1396, 1351, 1267, 1176, 1109, 1048, 924, 896, 754, 468, 369	
n-C_4H_9:[c]	250, 398, 433, 702, 788, 836, 928, 977, 1020, 1059, 1135, 1223, 1284, 1290, 1373, 1394, 1425, 1450, 1458, 1463, 1472, 2789, 2841, 2846, 2849, 2871, 2901, 2903, 2944, 3030	
CH_3:[32]	3184 (2), 3002, 1383(2), 580	
C_3H_8:[33]	2977, 2973, 2968(2), 2967, 2962, 2887(2), 1476, 1472, 1464, 1462, 1451, 1392, 1378, 1338, 1278, 1192, 1158, 1054, 940, 922, 869, 748, 369	
n-C_4H_{10}:[33]	1469, 1451 (2), 1381, 1359, 1151, 1052, 833, 429, 1464, 1258, 952, 728, 1462, 1300, 1180, 804, 244, 1487, 1378, 1295, 1012, 976, 2963, 2962 (3), 2909, 2900, 2880 (2), 2872, 2865	
n-C_5H_{12}:[33]	1486, 1458, 1446, 1379, 1332, 1148, 1042, 868, 400, 184, 1463, 1304, 1238, 981, 759, 1478, 1454, 1380, 1367, 1264, 1068, 1021, 927, 404, 1463, 1288, 1177, 857, 726, 2962, 2962, 2962, 2962, 2911, 2904, 2899, 2880, 2880, 2874, 2868, 2864	
	rotational constants (cm^{-1}), symmetry numbers (σ, number of minima in parentheses if different), and rotational barriers (kJ mol^{-1})	
C_2H_5:[a]	$B = 1.226$; $\sigma = 1$	
	$B_i = 15.19$; $\sigma = 6$; $V_0 = 0$	
n-C_3H_7:[b]	$B = 0.4361$; $\sigma = 2$	
	$B_{i1} = 10.39$; $\sigma = 2$; $V_0 = 0$	
	$B_{i2} = 6.282$; $\sigma = 3$; $V_0 = 14.0$	
n-C_4H_9:[c]	$B = 0.2331$; $\sigma = 1$	
	$B_{i1} = 6.256$; $\sigma = 3$; $V_0 = 14.25$	
	$B_{i2} = 1.644$; $\sigma = 1(3)$; $V_0 = 18.61$	(C2−C3 torsion)
	$B_{i3} = 10.47$; ó = 2; $V_0 = 0$	
CH_3:[32]	$B = 7.6036$; $\sigma = 6$	
C_3H_8:	$B = 0.9740$; $\sigma = 1$	(1-dimensional active)[34]
	$B = 0.2647$; $\sigma = 2$	(2-dimensional inactive)[34]
	$B_{i1,i2} = 6.102$; $\sigma = 3$, $V_o = 13.63$	(two CH_3 torsions, active)[35]
n-C_4H_{10}:[36,37]	$B = 0.736$; $\sigma = 1$	(1-dimensional active)
	$B = 0.1208$; $\sigma = 2$	(2-dimensional inactive)
	$B_{i1,i2} = 5.713$; $\sigma = 3$, $V_o = 13.43$	(two CH_3 torsions, active)
	$B_{i3} = 1.487$; $\sigma = 1(3)$, $V_o = 16.48$	(C2−C3 torsion, active)
n-C_5H_{12}:[36,37]	$B = 0.1317$; $\sigma = 2$	
	$B_{i1,i2} = 5.419$; $\sigma = 3$, $V_o = 13.43$	(two CH_3 torsions)
	$B_{i3,i4} = 1.317$; $\sigma = 1(3)$, $V_o = 11.04$	(C2−C3 and C3−C4 torsions)

[a] Properties of C_2H_5 are a combination of experimental data of Chettur and Snelson[38] and ab initio results of Quelch et al.[39] [b] Properties of *n*-C_3H_7 are from an ab initio study of Hu et al.[40] [c] Properties of *n*-C_4H_9 are from an ab initio study of Knyazev and Slagle.[16]

procedure was then repeated until convergence. Convergence (within less than 2%) was achieved for reaction 1 after three iterations and for reaction 2 after one iteration. Molecular properties such as heats of formation, vibrational frequencies, and rotational constants used in the calculations are listed in Table 2. The *ChemRate* program[41] was used in all calculations, including the calculations of the densities of states required to evaluate the $k(E)$ dependences via expression XII. Densities of states were calculated using the modified Beyer−Swinehart formalism[42,43] for harmonic oscillators and free rotors and the method of Knyazev[37] for hindered internal rotors. The method of Gaynor et al.[44] was used to solve the steady-state master equation. The exponential-down[21,45] model of collisional energy transfer was used.

It was assumed in the calculations that the experimental rate constants represent the recombination reaction channels. Although a minor (~4−6%)[46,47] contribution of disproportionation can be expected in reactions 1 and 2, the potential effects of neglecting these channels on the falloff modeling are negligible in the case of reaction 2 and far outweighed by the uncertainties of extrapolation to the high-pressure-limit in the case of reaction 1.

The choice of the collisional energy transfer parameter, $<\Delta E>_{down}$ (average energy transferred per deactivating collision with the bath gas)[21,45] can be important in such modeling if the reaction under study is far from the high-pressure-limit conditions. The $<\Delta E>_{down} = 0.8 \times (T/\text{K})$ cm^{-1} temperature dependence derived in our earlier work[6] from the results of Knyazev and Tsang[48] on modeling of the chemically and thermally activated decomposition of *sec*-C_4H_9 (with corrections for larger energy barrier) was used in the current study without modifications. Because these $<\Delta E>_{down}$ values have large uncertainties, calculations were also performed with the proportionality coefficient in the $<\Delta E_{down}$ vs T dependence changed by a factor of 2 in both directions in order to assess the effects of these uncertainties on the results of falloff modeling.

The values of the k/k^∞ falloff correction coefficients obtained in the modeling for reactions 1 and 2 are listed in Table 1. Relative uncertainties of extrapolation to the high-pressure limit were estimated as the differences (on a logarithmic scale) between the k/k^∞ values obtained using the $<\Delta E>_{down} = 0.8 \times (T/\text{K})$ cm^{-1} and the $<\Delta E>_{down} = 0.4 \times (T/\text{K})$ cm^{-1} formulas for the $<\Delta E>_{down}$ temperature dependence (A factor of 2 decrease in the coefficient of the $<\Delta E>_{down}$ vs T dependence results in a larger relative change in k/k^∞ than a similar increase does.). The final uncertainty values of the high-pressure-limit rate constants listed in Table 1 (presented as uncertainty factors) were obtained by adding the extrapolation uncertainties to the experimental ones.

As can be expected, the largest falloff corrections (smallest k/k^∞ values, 0.57−0.75) were obtained at the highest experimental temperature (800 K) for the reaction involving the

smallest species, reaction 1. At the same time, it was found that reaction 2 is very close to the high-pressure limit under all experimental conditions ($k/k^{\infty} \geq 0.97$ even with the $<\Delta E>_{down} = 0.4 \times (T/\mathrm{K})\ \mathrm{cm}^{-1}$ model). Thus, the uncertainty of extrapolation is significant only for reaction 1.

The high-pressure-limit rate constants of reaction 1 obtained by the above extrapolation of experimental results are displayed in Figure 2 (smaller open circles). As can be seen from the plot, the curvature of the Arrhenius plot observed when the experimental rate constant values are displayed disappears when corrections for the falloff effects are introduced. The temperature dependence of k_1^{∞} can be represented by the following expressions

$$k_1^{\infty} = 2.36 \times 10^{-11} \exp(433\ \mathrm{K}/T)\ \mathrm{cm}^3\ \mathrm{molecule}^{-1}\ \mathrm{s}^{-1} \quad \text{(IX)}$$

The estimated uncertainty of expression IX is 25% at temperatures 300−500 K and increases to a factor of 1.6 at 800 K. The falloff corrections for reaction 2 are very minor and, thus, the corrected expression for the high-pressure-limit rate constant (X) differs very little from expression V obtained with uncorrected experimental data

$$k_2^{\infty} = 3.06 \times 10^{-11} \exp(387\ \mathrm{K}/T)\ \mathrm{cm}^3\ \mathrm{molecule}^{-1}\ \mathrm{s}^{-1} \quad \text{(X)}$$

The estimated uncertainty of the k_2^{∞} vs T dependence given by formula X is 25%. The temperature dependence of the high-pressure-limit rate constant of reaction 3 is given by expression VI.

IV. Discussion

This work presents the first direct determination of the rate constants of reactions 1−3 as functions of temperature. Absolute values of rate constants have been reported before only for reaction 1 at room temperature.[5,7,8] Figure 2 presents the results of the current investigation in comparison with those of the earlier studies. As can be seen from the plot, our room-temperature value of k_1 is in agreement with that of Garland and Bayes. The values of Anastasi and Arthur and of Sillesen et al., however, are substantially lower than the results of the current work.

Anastasi and Arthur[7] used molecular modulation spectrometry at a pressure of 131 Torr of nitrogen/azomethane/azoethane bath gas and obtained the value of $k_1 = (4.7 \pm 0.4) \times 10^{-11}$ cm^3 molecule^{-1} s^{-1}. In these experiments, radicals were created by a square-wave photolysis of suitable precursors and the values of the rate constants were derived from the in-phase and the in-quadrature absorption signals of radicals. The results relied on the validity of the assumed kinetic mechanism. It should be mentioned that the validity of the results is somewhat undermined by the fact that the room-temperature rate constant of the recombination of CH_3 radicals obtained in the same work, 3.5×10^{-11} cm^3 molecule s^{-1}, is lower (by nearly a factor of 2) than the currently accepted value[20,47,49,50] of $\sim 6.0 \times 10^{-11}$ cm^3 molecule s^{-1} derived from direct experiments. As the authors of ref 7 pointed out, the values of the CH_3 and C_2H_5 recombination rates had a strong influence on the derived rates of cross-combination reactions.

The most direct prior determination of the rate constant of reaction 1 ($C_2H_5 + CH_3$) is that of Garland and Bayes[5] who studied reaction 1 among several other cross-radical reactions using a laser photolysis/photoionization mass spectrometry method similar to the one employed in the current investigation. These authors used literature values of the rate constants of the $CH_3 + CH_3$ reaction to evaluate initial CH_3 radical concentrations. Thus, the resultant k_1 value ($(9.3 \pm 4.2) \times 10^{-11}$ cm^3 molecule^{-1} s^{-1}) was dependent on the accuracy of the radical recombination rate constant used by the authors.

Sillesen et al. used pulsed radiolysis of H_2 with spectroscopic detection of CH_3 and kinetic modeling to study the system of consecutive reactions $H + C_2H_4 \rightarrow C_2H_5$, $H + C_2H_5 \rightarrow 2CH_3$, $C_2H_5 + CH_3 \rightarrow$ products. The value of $k_1 = (6.6 \pm 0.3) \times 10^{-11}$ cm^3 molecule^{-1} s^{-1} was derived in this work from modeling the $[CH_3]$ vs time profiles using an assumed chemical mechanism and literature values of the rate constants of other reactions. The result thus depended on the accuracy of the kinetic mechanism and the rate constants of other reactions used in the model.

Garland and Bayes[5] used their experimental data on radical cross reactions to test the validity of the "geometric mean rule"[3−5]

$$k_{AB} = 2(k_{AA}k_{BB})^{1/2} \quad \text{(XI)}$$

frequently used to estimate rate constants of cross radical reactions (k_{AB}) of the type A + B from the values of k_{AA} and k_{BB}, the rate constants of the A + A and B + B self-reactions. Such a comparison is also performed in the current work. It is, however, restricted to reactions 1 and 2 at room temperature because no data are available on the rates of *n*-C_4H_9 radicals self-reaction and direct experiments on the rates of self-reactions of ethyl[51,52] and *n*-propyl radicals[53] have been performed only at room temperature.

The rate constants of methyl radical self-reaction

$$CH_3 + CH_3 \rightarrow C_2H_6 \quad (8)$$

are well-known. Two recent "global fits"[49,50] of falloff data provide parametrization for the rate constants that differ very little (less than 5%) in the high-pressure limit. Most of the experimental data used in these parametrizations come from the experimental study of Slagle et al.[20] who used the experimental technique and the apparatus employed in the current work. These authors reported a ± 20% uncertainty in their experimental rate constant values. Thus, in the calculations according to the "geometric mean rule," we used the parametrization of Hessler and Ogren[50] ($k_8^{\infty}(298\ \mathrm{K}) = 5.81 \times 10^{-11}$ cm^3 molecule^{-1} s^{-1}) with 20% uncertainty.

The most direct, real-time kinetic measurements of the rate constant of the self-reaction of ethyl radicals

$$C_2H_5 + C_2H_5 \rightarrow \text{products} \quad (13)$$

are those of Adachi et al.[51] and Atkinson and Hudgens.[52] Adachi et al. used flash photolysis of azoethane to produce C_2H_5 and monitored their decay due to reaction 13 by absorption spectroscopy. Atkinson and Hudgens used photolysis of Cl_2 followed by the rapid reaction of Cl atoms with ethane to produce ethyl radicals and monitored their decay by the cavity ring-down method. The rate constants of reaction 13 reported by these two groups ($(2.33 \pm 0.45) \times 10^{-11}$ [51] and $(1.99 \pm 0.44) \times 10^{-11}$ [52] cm^3 molecule^{-1} s^{-1}) are higher than those obtained by the molecular modulation spectroscopy method (1.5×10^{-11} [54] and 1.7×10^{-11} [7] cm^3 molecule^{-1} s^{-1}). We use the value of Adachi et al. because it was obtained in direct real-time experiments. The value of ref 52, although also obtained in direct real-time measurements, could potentially have been affected by the very fast chain reaction ensuing from the photolysis of Cl_2 in the presence of large concentrations of C_2H_6

$$C_2H_5 + Cl_2 \rightarrow C_2H_5Cl + Cl \quad (14)$$

$$k_{14}\,(298\ \mathrm{K}) = 2.1 \times 10^{-11}\ \mathrm{cm^3\ molecule^{-1}\ s^{-1}}$$ [55]

$$Cl + C_2H_6 \rightarrow HCl + C_2H_5 \quad (15)$$

$$k_{15}\,(298\ \mathrm{K}) = 5.9 \times 10^{-11}\ \mathrm{cm^3\ molecule^{-1}\ s^{-1}}$$ [56]

The only absolute value of the rate constant of the self-reaction of *n*-C_3H_7 radicals

$$n\text{-}C_3H_7 + n\text{-}C_3H_7 \rightarrow \text{products} \quad (16)$$

available in the literature is that of Adachi and Basco[53] ($k_{16} = (1.98 \pm 0.33) \times 10^{-11}$ cm^3 molecule^{-1} s^{-1}) obtained by the flash photolysis/absorption spectroscopy technique.

The resultant k_1 and k_2 values calculated via eq XI (the "geometric mean rule") using the literature values of k_8, k_{13}, and k_{16} are $k_1 = (7.3 \pm 1.5) \times 10^{-11}$ and $k_2 = (6.8 \pm 1.2) \times 10^{-11}$ cm^3 molecule^{-1} s^{-1}. The upper and lower limiting values were calculated using the upper and lower limits of k_8, k_{13}, and k_{16}. The calculated value of k_1 is in reasonable agreement with the average room-temperature experimental value obtained in this work, $k_1(298\ \mathrm{K}) = (9.8 \pm 2.7) \times 10^{-11}$ cm^3 molecule^{-1} s^{-1}. The calculated value of k_2, however, is lower than the experimental room-temperature value $k_2(298\ \mathrm{K}) = (11.2 \pm 2.5) \times 10^{-11}$ cm^3 molecule^{-1} s^{-1}, the difference being larger than the combined uncertainties. The experimental uncertainties of k_1, k_2, k_8, k_{13}, and k_{16} do not allow a more certain assessment of the validity of the "geometric mean rule" as applied to reactions 1 and 2. The disagreement between the experimental and calculated values of k_2 may lead to the conclusion of inadequacy of the "geometrical mean rule"; however, one should keep in mind that this conclusion would critically depend on the accuracy of the rate constant value used for the *n*-propyl radical self-reaction (k_{16}), which is the result of the room-temperature measurement of only one group.

The values of k_1^∞, k_2^∞, and k_3^∞ obtained in the current work, combined with the known thermochemistry of reactions 1−3 (Table 2), can be used to evaluate the high-pressure-limit rate constants of the reverse reactions of decomposition of propane, *n*-butane, and *n*-pentane. The decomposition rate constants values can be represented with the expressions

$$k_{-1}^\infty(T) = 1.7 \times 10^{17}\exp(-44\,000\ \mathrm{K}/T)\ \mathrm{s^{-1}}\ (301-800\ \mathrm{K}) \quad (XII)$$

$$k_{-2}^\infty(T) = 2.8 \times 10^{17}\exp(-44\,300\ \mathrm{K}/T)\ \mathrm{s^{-1}}\ (297-600\ \mathrm{K}) \quad (XIII)$$

$$k_{-3}^\infty(T) = 1.8 \times 10^{17}\exp(-44\,100\ \mathrm{K}/T)\ \mathrm{s^{-1}}\ (301-520\ \mathrm{K}) \quad (XIV)$$

evaluated for the experimental temperature ranges of this work as indicated in parentheses. The uncertainty of expression XII changes from a factor of 6 at room temperature to factors of 4 at 400 K, 2.7 at 600 K, and 2.2 at 800 K. The uncertainties of expressions XIII and XIV are equal to factors of 4.6 at room temperature, 3.1 at 400 K, 2.5 at 500 K, and 2.1 at 600 K. These uncertainties originate primarily in the error limits of the heats of formation of the involved species (overall uncertainties in the reaction enthalpy values are 3.0 kJ mol^{-1} for reaction 1 and 3.8 kJ mol^{-1} for reactions 2 and 3, see Table 2). In the calculations of the equilibrium and the decomposition rate constants, it was assumed that the values of the rate constants of the R + CH_3 reactions obtained in the current study represent only recombination and minor disproportionation channels (4−6%[46,47]) were neglected.

Acknowledgment. This research was supported by Division of Chemical Sciences, Office of Basic Energy Sciences, Office of Energy Research, U.S. Department of Energy under Grant No. DE-FG02-94ER1446.

References and Notes

(1) Tsang, W.; Hampson, R. F. *J. Phys. Chem. Ref. Data* **1986**, *15*, 1087.
(2) Warnatz, J. In *Combustion Chemistry*; Gardiner, W. C., Jr., Ed. Springer-Verlag: New York, 1984.
(3) Kerr, J. A.; Trotman-Dickenson, A. F. *Prog. React. Kinet.* **1961**, *1*, 105.
(4) Blake, A. R.; Henderson, J. F.; Kutschke, K. O. *Can. J. Chem.* **1961**, *39*, 1920.
(5) Garland, L. J.; Bayes, K. D. *J. Phys. Chem.* **1990**, *94*, 4941.
(6) Knyazev, V. D.; Slagle, I. R. *J. Phys. Chem. A* **2001**, *105*, 3196.
(7) Anastasi, C.; Arthur, N. L. *J. Chem. Soc., Faraday Trans. 2* **1987**, *83*, 277.
(8) Sillesen, A.; Ratajczak, E.; Pagsberg, P. *Chem. Phys. Lett.* **1993**, *201*, 171.
(9) Slagle, I. R.; Gutman, D. *J. Am. Chem. Soc.* **1985**, *107*, 5342.
(10) Stoliarov, S. I.; Knyazev, V. D.; Slagle, I. R. *J. Phys. Chem. A* **2000**, *104*, 9687.
(11) Krasnoperov, L. N.; Niiranen, J. T.; Gutman, D.; Melius, C. F.; Allendorf, M. D. *J. Phys. Chem.* **1995**, *99*, 14 347.
(12) Daly, N. R. *Rev. Sci. Insrum.* **1960**, *31*, 264.
(13) Lightfoot, P. D.; Kirwan, S. P.; Pilling, M. J. *J. Phys. Chem.* **1988**, *92*, 4938.
(14) Seetula, J. A.; Russell, J. J.; Gutman, D. *J. Am. Chem. Soc.* **1990**, *112*, 1347.
(15) Bencsura, A.; Knyazev, V. D.; Xing, S.-B.; Slagle, I. R.; Gutman, D. *Symp. Int. Combust. Proc.* **1992**, *24*, 629.
(16) Knyazev, V. D.; Slagle, I. R. *J. Phys. Chem.* **1996**, *100*, 5318.
(17) Niiranen, J. T.; Gutman, D. *J. Phys. Chem.* **1993**, *97*, 9392.
(18) Bevington, P. R. *Data Reduction and Error Analysis for the Physical Sciences*; McGraw-Hill: New York, 1969.
(19) Feng, Y.; Niiranen, J. T.; Bencsura, A.; Knyazev, V. D.; Gutman, D.; Tsang, W. *J. Phys. Chem.* **1993**, *97*, 871.
(20) Slagle, I. R.; Gutman, D.; Davies, J. W.; Pilling, M. J. *J. Phys. Chem.* **1988**, *92*, 2455.
(21) Gilbert, R. G.; Smith, S. C. *Theory of Unimolecular and Recombination Reactions*; Blackwell: Oxford, 1990.
(22) Holbrook, K. A.; Pilling, M. J.; Robertson, S. H. *Unimolecular Reactions*, 2nd ed.; Wiley: New York, 1996.
(23) Forst, W. *Theory of Unimolecular Reactions*; Academic Press: New York, 1973.
(24) Robinson, P. J.; Holbrook, K. A. *Unimolecular Reactions;* Wiley-Interscience: New York, 1972.
(25) Kerr, J. A. *CRC Handbook of Chemistry and Physics*; Lide, D. R., Ed.; CRC Press: Boca Raton, Florida, U.S.A., 1994−1995.
(26) Seakins, P. W.; Pilling, M. J.; Niiranen, J. T.; Gutman, D.; Krasnoperov, L. N. *J. Phys. Chem.* **1992**, *96*, 9847.
(27) Seetula, J. A.; Slagle, I. R. *J. Chem. Soc. Faraday Trans.* **1997**, *93*, 1709.
(28) Russell, J. J.; Seetula, J. A.; Senkan, S. M.; Gutman, D. *Int. J. Chem. Kinet.* **1988**, *20*, 759.
(29) Dobis, O.; Benson, S. W. *Int. J. Chem. Kinet.* **1987**, *19*, 691.
(30) Pittam, D. A.; Pilcher, G. *J. Chem. Soc., Faraday Trans. 1* **1972**, *68*, 2224.
(31) Prosen, E. J.; Maron, F. W.; Rossini, F. D. *J. Res. NBS* **1951**, *46*, 106.
(32) Chase, M. W., Jr. *J. Phys. Chem. Ref. Data* **1998**, *Monograph 9*, 1.
(33) Shimanouchi, T. *Tables of Molecular Vibrational Frequencies. Consolidated Volume, I.*; National Bureau of Standards: Gaithersburg, MD, 1972.
(34) Lide, D. R., Jr. *J. Chem. Phys.* **1960**, *33*, 1514.
(35) Durig, J. R.; Groner, P.; Griffin, M. G. *J. Chem. Phys.* **1977**, *66*, 3061.
(36) Gang, J.; Robertson, S. H.; Pilling, M. J. *J. Chem. Soc., Faraday Trans.* **1996**, *92*, 3509.
(37) Knyazev, V. D. *J. Phys. Chem. A* **1998**, *102*, 3916.
(38) Chettur, G.; Snelson, A. *J. Phys. Chem.* **1987**, *91*, 3483.
(39) Quelch, G. E.; Gallo, M. M.; Schaefer, H. F., III *J. Am. Chem. Soc.* **1992**, *114*, 8239.
(40) Hu, W.-P.; Rossi, I.; Corchado, J. C.; Truhlar, D. G. *J. Phys. Chem. A* **1997**, *101*, 6911.

(41) Mokrushin, V.; Bedanov, V.; Tsang, W.; Zachariah, M. R.; Knyazev, V. D. *ChemRate, Version 1.16*; National Institute of Standards and Technology: Gaithersburg, MD 20899, USA, 1999.

(42) Beyer, T.; Swinehart, D. F. *Comm Assoc. Comput. Machines* **1973**, *16*, 379.

(43) Astholz, D. C.; Troe, J.; Wieters, W. *J. Chem. Phys* **1979**, *70*, 5107.

(44) Gaynor, B. J.; Gilbert, R. G.; King, K. D. *Chem. Phys. Lett* **1978**, *55*, 40.

(45) Rabinovitch, B. S.; Tardy, D. C. *J. Chem. Phys.* **1966**, *45*, 3720.

(46) Tsang, W. *J. Phys. Chem. Ref. Data.* **1988**, *17*, 887.

(47) Baulch, D. L.; Cobos, C. J.; Cox, R. A.; Esser, C.; Frank, P.; Just, Th.; Kerr, J. A.; Pilling, M. J.; Troe, J.; Walker, R. W.; Warnatz, J. *J. Phys. Chem. Ref. Data* **1992**, *21*, 411.

(48) Knyazev, V. D.; Tsang, W. *J. Phys. Chem. A* **2000**, *104*, 10 747.

(49) Robertson, S. H.; Pilling, M. J.; Baulch, D. L.; Green, N. J. B. *J. Phys. Chem.* **1995**, *99*, 13 452.

(50) Hessler, J. P.; Ogren, P. J. *J. Phys. Chem.* **1996**, *100*, 984.

(51) Adachi, H.; Basco, N.; James, D. G. L. *Int. J. Chem. Kinet.* **1979**, *11*, 995.

(52) Atkinson, D. B.; Hudgens, J. W. *J. Phys. Chem. A* **1997**, *101*, 3901.

(53) Adachi, H.; Basco, N. *Int. J. Chem. Kinet.* **1981**, *13*, 367.

(54) Parkes, D. A.; Quinn, C. P. *J. Chem. Soc., Faraday Trans. 1* **1976**, *72*, 1952.

(55) Timonen, R. S.; Gutman, D. *J. Phys. Chem.* **1990**, *86*, 2987.

(56) Atkinson, R.; Baulch, D. L.; Cox, R. A.; Hampson, R. F., Jr.; Kerr, J. A.; Rossi, M. J.; Troe, J. *J. Phys. Chem. Ref. Data* **1997**, *26*, 521.

(57) Good, W. D. *J. Chem. Thermodyn.* **1970**, *2*, 237.